Supporting information for: Electrostatic Binding and Hydrophobic Collapse of Peptide-Nucleic Acid Aggregates Quantified Using Force Spectroscopy

Joan Camunas-Soler,[†,‡] Silvia Frutos,[†,‡] Cristiano V. Bizarro,[†,‡,@] Sara de Lorenzo,[†,‡] Maria Eugenia Fuentes-Perez,[¶] Roland Ramsch,[§,‡] Susana Vilchez,[§,‡] Conxita Solans,[§,‡] Fernando Moreno-Herrero,[¶] Fernando Albericio,[‖,‡,⊥,#] Ramón Eritja,[§,‖,‡] Ernest Giralt,[‖,‡] Sukhendu B. Dev,[‖] and Felix Ritort[*,†,‡]

Small Biosystems Lab, Departament de Física Fonamental, Universitat de Barcelona, Avda. Diagonal 647, 08028 Barcelona, Spain, CIBER de Bioingeniería, Biomateriales y Nanomedicina, Instituto de Salud Carlos III, Madrid, Spain, Centro Nacional de Biotecnología, CSIC, 28049 Cantoblanco, Madrid, Spain, Institut de Química Avançada de Catalunya, Consejo Superior de Investigaciones Científicas (IQAC-CSIC), 08034 Barcelona, Spain, Institute for Research in Biomedicine (IRB Barcelona), Barcelona Science Park, Baldiri Reixac 10-12, 08028 Barcelona, Spain, Department of Organic Chemistry, University of Barcelona, 08028. Barcelona, Spain, and School of Chemsitry and Physics, University of KwaZulu-Natal, 4001-Durban, South Africa

E-mail: fritort@gmail.com

Contents

*To whom correspondence should be addressed

†Small Biosystems Lab, Departament de Física Fonamental, Universitat de Barcelona, Avda. Diagonal 647, 08028 Barcelona, Spain

‡CIBER de Bioingeniería, Biomateriales y Nanomedicina, Instituto de Salud Carlos III, Madrid, Spain

¶Centro Nacional de Biotecnología, CSIC, 28049 Cantoblanco, Madrid, Spain

§Institut de Química Avançada de Catalunya, Consejo Superior de Investigaciones Científicas (IQAC-CSIC), 08034 Barcelona, Spain

‖Institute for Research in Biomedicine (IRB Barcelona), Barcelona Science Park, Baldiri Reixac 10-12, 08028 Barcelona, Spain

⊥Department of Organic Chemistry, University of Barcelona, 08028. Barcelona, Spain

#School of Chemsitry and Physics, University of KwaZulu-Natal, 4001-Durban, South Africa

@Current Address: Centro de Pesquisas em Biologia Molecular e Funcional/PUCRS Avenida Ipiranga 6681, Tecnopuc, Partenon 90619-900, Porto Alegre, RS, Brazil

S1 Supplementary Methods

S1.1 Optical tweezers experiments

S1.1.1 Stretching experiments with dsDNA

For the dsDNA stretching experiments, 1 μl of a $\sim$ 0.5 pmol/ml dilution of a 24-kb dsDNA stock solution (see Section S1.2) was mixed and incubated for 30' with 5 μl antidigoxigenin-coated beads (0.5% w/v, 3.15 μm diameter) and 14 μl TE (Tris 10 mM, EDTA 1 mM, 0.01% NaN_3, pH7.5) 500 mM NaCl. The sample was then diluted to 1 ml in TE 100 mM NaCl, 0.1 mg/ml BSA (New England Biolabs). The sample was incubated at least 30 min with BSA before starting the experiments to passivate the bead surface. A sample of streptavidin-coated beads was also prepared by diluting 1 μl of beads (0.5% w/v, 1.87 μm diameter, Kisker Biotech) in 1 ml TE 100 mM NaCl, 0.1 mg/ml BSA. Beads were differentially flowed into the fluidics chamber through lateral channels, and a dsDNA tether between an optically trapped bead and a pipette-subjected bead was created as previously described.

The molecule was submitted to several stretch/relaxation cycles up to a maximum pulling force of 45 pN and a minimum molecular extension of $\sim$ 4.5 μm to characterize its elastic properties. At least three consecutive pulling cycles were fitted to the Inextensible Worm-Like Chain (WLC) in the low-force regime (F$\leq$5 pN), and to the extensible WLC in the high-force regime (F$\leq$40 pN).

After flowing KF, the low-force region (F$\leq$5 pN) of the release cycles was still well described by the inextensible WLC model. The contour length and persistence length of the molecule were then obtained as an average of at least four pulling cycles. Higher force-data was not used for the fits, as data is not well described by the extensible WLC model after flowing KF.

For the experiments in which KF was flowed without keeping the molecule at a constant force, the DNA was maintained at an end-to-end distance of 6 μm (flow-rate: 9 μl/min). This corresponds to a drag force on the trapped bead of $\sim$14 pN perpendicularly to the stretching direction. In these experiments the flow was stopped after 5, 15 and 30 min and stretching curves were collected at a pulling speed of 500 nm/s.

For the constant force experiments a lower flow-rate of 3 μl/min was used to maintain the overall tension on the DNA molecule similar to the force on the stretching direction. This buffer flow corresponds to a drag force of $\sim$4 pN perpendicular to the stretching direction. To accurately perform the constant force experiments at 1 pN, we flowed KF keeping the DNA molecule at a higher tension of 3 pN. Once the chamber was fully equilibrated the flow was stopped and the force set at 1 pN.

S1.1.2 DNA unzipping experiments

For the DNA unzipping experiments a 6.8-kb DNA hairpin sample (see Section S1.2) was tethered by bringing the bead in the optical trap in close contact to the bead on the micropipette due to the short length of the hairpin handles. The DNA and beads incubations were prepared following the same protocol as for the DNA stretching experiments, the only difference being the specific DNA concentration required to optimize the tethering of a single DNA molecule between beads. The DNA hairpin was then fully unzipped in TE 100 mM NaCl at a pulling rate of 50 nm/s, and maintained at a position in which at least half of the hairpin stem remained unzipped. The molecule was then rinsed with KF for at least 3 min (flow-rate: 9 μl/min). The peptide flow was then stopped and unzipping/rezipping curves recorded.

S1.1.3 Experiments with ssDNA

For the ssDNA experiments a 6.8-kb DNA hairpin was prepared and tethered as for the unzipping experiments. The tethered hairpin was fully unzipped in a buffer (TE 100 mM NaCl) that contains a 250 nM concentration of a 30-base oligonucleotide complementary to the loop and its flanking region (see Table S2 for oligonucleotide sequence, oligo name: Blockloop30). The annealing of an oligonucleotide to the tethered hairpin stabilizes the ssDNA form over the dsDNA form down to forces close to 1 pN. The elastic response of the ssDNA molecules was then recorded at a pulling rate of 100 nm/s in the force range 5 pN $<$ F $<$ 20 pN and characterized by means of the FJC model (see Section Section S5). Then, the molecule was maintained at a constant force by means of the

force-feedback while a freshly prepared 40 μM KF solution was flowed (flow-rate: 3 μl/min).

S1.2 DNA substrates preparation

For the DNA stretching experiments we prepared a 24508-bp DNA molecule with biotin and digoxigenin tags at the 3'-ends of the molecule. The DNA template was prepared by cleaving N6-methyladenine free λ-DNA (New England Biolabs) with *Xba*I restriction enzyme, and purified using Wizard DNA clean-up system kit (Promega). The digoxigenin tag was prepared by annealing to the cosL end of λ-DNA an oligonucleotide tailed at its 3'-end with digoxigenin-labeled dUTP's using terminal transferase (Roche). The biotin tag was prepared by annealing two complementary oligonucleotides designed to create an *Xba*I cohesive end at one side. One of the oligonucleotides was tailed at its 3'-end with multiple biotins with biotin-labeled dUTP's using terminal transferase (Roche). Oligonucleotides were purified after tailing steps using the QIAquick Nucleotide Removal Kit (Qiagen). The digoxigenin tag was annealed to the half λ-DNA molecule by incubation for 10 min at 68°*C* in a 10-fold excess oligonucleotide. Then, the biotin tag was annealed by incubation for 1h at 42°*C* (using 20-fold excess oligonucleotides) followed by cooling down to room temperature. Ligation was performed as an overnight reaction at 16°*C* using T4 DNA ligase (New England Biolabs).

For the DNA unzipping experiments a 6838-bp DNA hairpin with a tetraloop at one end and two 29-bp dsDNA handles at the other end was prepared. The synthesis is based on a previously described method[S1] but was modified to introduce double digoxigenin and biotin tags at each handle to enhance tether lifetimes (Figure S8). Briefly, N6-methyladenine free λ-DNA (New England Biolabs) was digested with *Bam*HI, phosphorylated at its 5'-ends with T4 polynucleotide kinase (New England Biolabs), and purified using Wizard SV Gel and PCR clean-up system (Promega). The 6770-bp restriction fragment contained between positions 41733 and 48502 (cosR end) was used as the stem of the DNA hairpin. To create the end-loop of the molecule, the stem was annealed to an oligonucleotide (BamHI-loop2) that self-assembles in a hairpin structure with a tetraloop at one end, and an overhang complementary to the *Bam*HI restriction site on the other end. To cre-

ate the dsDNA handles, we used two partially complementary oligonucleotides (cosRlong and Bio-cosRshort3) that hybridize forming a protruding end complementary to the cosR end. The Bio-cosRshort3 oligonucleotide was purchased 5'-biotinylated, and the cosRlong oligonucleotide was tailed with multiple digoxigenins at its 3'-end as previously explained. To create the doubly biotynilated dsDNA handle, a third oligonucleotide (splint3) complementary to the unpaired regions of BIO-cosRshort3 was purchased and tailed at its 3' end with multiple biotins with biotin-labeled dUTP's using terminal transferase (Roche). To create the digoxigenin dsDNA handle we used a modified oligonucleotide (inverted-splint, Thermo Scientific) complementary to the unpaired region of cosRlong. This oligonucleotide contains two modifications: a C3 spacer at its 3' end to block this end in tailing reactions, and a polarity inversion at its 5' end using a 5'-5' linkage. This end can therefore be tailed with digoxigenin-labeled dUTP's using terminal transferase (Roche). In this way, both ends of the handle could be tailed with multiple digoxigenins (Figure S8). Oligonucleotides were purified after tailing steps using the Qiaquick Nucleotide Removal Kit (Qiagen). The oligonucleotides were annealed to the 6770-bp stem by incubation for 10 min at $70°C$, followed by incubation for 10 min at $55°C$ and cooling down to room temperature. Ligation was performed as an overnight reaction at $16°C$ using T4 DNA ligase (New England Biolabs).

The sequence of the oligonucleotides used for the hairpin synthesis, together with the 30-base oligonucleotide used to generate the ssDNA template are specified in Table S2.

S1.3 Kahalalide F sample preparation

Stock solutions containing 2 mM KF were prepared by dissolving a $\sim$1-2 mg sample of pure lyophylized Kahalalide F (gently provided by Pharmamar) in 100% DMSO (Sigma, Molecular Biology Grade). Stock solutions were then vortexed at low speed for 20 min and filtered with a 0.2 μm pore PTFE membrane filter (Millipore) that was pre-rinsed with 300 μl DMSO to reduce filter extractables. Sample concentration after stock filtration was verified by means of HPLC: An aliquot before and after filtering was collected and stored in ACN:H20 (50:50). These samples were sequentially processeÄd in an HPLC using a 5%-100% acetonitrile gradient. The elution

peak was monitored at 220 nm, and the integrated area was compared between both samples. No sample loss happened during filtration (Figure S9). Ready-to-use Kahalalide F stock solutions were stored at -20°C as 20-60 μl aliquots. To prepare diluted working solutions, a stock solution aliquot was thawed and sequentially diluted in TE 100 mM NaCl (*e.g.* 40 μM). The final DMSO concentration was always adjusted to 2%. Once thawed, stock solutions were not stored again to avoid the problems related to freeze-thaw cycles.[S2,S3] Samples were always prepared in glass vials, and a glass syringe used for sample filtering. Use of glass material was preferred to avoid material leaching from disposable plasticware,[S4] and the good performance of glass infusion devices for low concentration samples of KF in clinical practice.[S5]

A mass spectrum of a 40 μM KF sample in 100 mM NH4OAc buffer pH7.0 (2% DMSO) is shown in Figure S10. The concentration of NH4OAc was set to obtain an ionic strength comparable to that used in the optical tweezers experiments.

S1.3.1 Mass Spectrometry Methods

Sample are introduced using an Automated Nanoelectrospray. Triversa NanoMate (Advion Bio-Sciences, Ithaca, NY, USA) sequentially aspirated the sample from a 384-well plate with disposable, conductive pipette tips, and infused it through the nanoESI Chip, which consists of 400 nozzles in a 20x20 array. Spray voltage was 1.75 kV and delivery pressure was 0.5 psi. Mass Spectrometer: Synapt HDMS (Waters, Manchester, UK). Samples were acquired with Masslynx software v.4 SCN 639 (Waters). **MS Conditions for TOF results:** NanoESI. Positive mode TOF. V mode. Sampling cone: 20 V. Source temperature: 20°C. Trap Collision Energy: 10. Transfer Collision Energy: 10. Trap Gas Flow: 8 ml/min. Vacuum Backing pressure: 5.89 mbar. m/z range: 300 to 5000, 500-15000. Instrument calibrated with CsI (external calibration). **MS Conditions for Ion Mobility results:** NanoESI. Positive mode Ion Mobility mode. V mode. Sampling cone: 20 V. Source temperature: 20°C. Trap Collision Energy: 10. Transfer Collision Energy: 10. Trap Gas Flow: 8 ml/min. IMS Wave Velocity: 300 m/s. IMS Wave Height: 9.5 V. Transfer Wave Velocity: 200 m/s. Transfer Wave Height: 8 V. Vacuum Backing pressure: 5.89 mbar. m/z range: 300 to

5000, 500-15000. Instrument calibrated with CsI (external calibration).

S1.4 Dynamic Light Scattering Methods

A Photon Correlation Spectrometer (PCS) 3D from LS INSTRUMENTS was used for DLS measurements. The instrument is equipped with a He-Ne laser (632.8 nm). Measurements of at least 90 s were recorded at an angle of 90°. The hydrodynamic radius was calculated by a manual exponential fitting of the first cumulant parameter. Standard deviations were calculated from the second cumulant. The measurement temperature of $25°C$ was maintained by a decaline bath, which matches the refractive index of glass and does not therefore interfere with the measurement. The evolution of the hydrodynamic radius was observed during 1 hour. The time indicated corresponds to the minutes past after preparation of the sample and the beginning of the measurement.

Zeta potential measurements were carried out at $25°C$ with a Malvern Instrument Zetasizer Nano Z by laser Doppler electrophoresis. Disposable polystyrene cells were used. Solutions of peptide, DNA and the mixture were measured at the same concentration as the light scattering measurements were performed. Commercially available λ-DNA (New England Biolabs) was used for the experiments.

S2 DLS measurements of KF and KF-DNA complexes

To characterize the size of KF aggregates we performed DLS measurements. The hydrodynamic radius of KF particles one minute after sample preparation was 170±20 nm (Figure S11**a**, red) and showed a high polydispersity. The hydrodynamic radius increased linearly with time with a growing rate of 3.2±0.6 nm/min, indicative of a rate of aggregation proportional to the surface of the aggregate. We attribute such growth to the hydrophobic interactions between peptides. However, the hydrodynamic radius of KF-DNA mixtures remained constant within experimental errors during 60 min after sample preparation (Figure S11**a**, black). This may be explained by the stabilizing effect induced by the added DNA. In fact, the average size of the particles could be

stabilized by adding DNA at a latter time-stage (Figure S11**b**, arrow). DNA as a strongly charged polyelectrolyte interacts with the positive charge of KF and might form an anionic, water-soluble shell around the peptide. We measured the zeta potential of KF particles finding a low positive value (Table S1) in agreement with the single positively charged residue of the peptide. A higher negative value was obtained for KF-DNA mixtures. KF oligomerization was also observed with size-exclusion HPLC (Figure S12).

S3 Simulation of KF-DNA stretching experiments

As described in the main text, KF-DNA stretching curves are simulated using a set of N non-interacting two-states systems (Figure 4**d**, Inset) that describe the contacts made between KF and DNA. Each contact can be in two conformations: formed or dissociated. The formed and dissociated states of contact i^{th} have extensions corresponding to 0 and x_i respectively. Initially the N contacts are found in the formed conformation. As the DNA is stretched and the force increased, the tilting of the free-energy landscape towards larger extensions favors the dissociated conformation, releasing an extension x_i.

The parameters that best reproduce the experimental force-extension curves are described in the main text. A set of figures in which a different parameter is modified in each panel (the others being kept at the optimal value) is presented in Figure S13**a-d**. In each panel, the optimal simulation is presented in black, whereas simulations with varying values of the modified parameters are presented in colors.

For $\Delta G_0 \leq 5\ k_BT$ most of the contacts remain in the dissociated conformation (60% for $\Delta G_0 = 5\ k_BT$) at the end of a simulated pulling cycle (minimum extension of $\sim 4.5\ \mu$m). This high fraction of dissociated contacts cannot explain the sawtooth pattern observed in the force-extension curve (FEC) in subsequent pulls. This suggests that a value of $\Delta G_0 \leq 5\ k_BT$ is too low to reproduce the experimental curves. On the other hand, for $\Delta G_0 \sim 10\ k_BT$ more than 90% of the contacts are formed again at the end of a pulling cycle (minimum extension of $\sim 4.5\ \mu$m), in agreement

with the experimental results both at low (50 nm/s) and high pulling speeds (500 nm/s). Finally, for free energies greater than 15 k_BT a sawtooth pattern is also observed in the relaxation curve, in disagreement with the releasing part of the observed experimental FEC for the same range of pulling speeds (Figure S13**a**).

Experimental force-extension curves show a broad distribution of rupture forces with most rupture events occurring at forces lower than 20 pN, but with a large rightmost tail (Figure S5**a**). This phenomenology can be well reproduced by considering: (i) that the transition state is close to the formed conformation (Figure S13**b**); and (ii) that the process is characterized by a disordered ensemble of barriers rather than a single valued barrier. This structural disorder is introduced in the form of an exponential distribution of barriers with a rightmost exponential tail of width $w' \geq 1\ k_BT$ (Figure S13**c**).

To model the experimental force-extension curves, we have assumed that the distribution of released lengths (x_i) follows the experimental distribution shown in Figure 4**b**. In Figure S13**d** a simulation using the experimental distribution is compared to simulations in which the system is characterized by a single contact length (x_i) rather than an exponential distribution. Finally the optimal distributions for the different parameters of the simulation are shown in Figure S13**e**.

S4 Measurement of tether stiffness from trap-distance fluctuations

A bead confined in an optical trap fluctuates around its equilibrium position due to thermal fluctuations. By the equipartition theorem the fluctuations of the bead position along the stretching direction are directly related to the effective stiffness of the system formed by the tethered molecule and the optical trap:[S6]

$$< \delta y^2 > = < y^2 > - < y >^2 = \frac{k_BT}{k_{\text{trap}} + k_{\text{mol}}} \quad . \tag{S1}$$

In an ideal force-feedback the stiffness of the trap vanishes and the bead fluctuations are only determined by the stiffness of the tether:

$$< \delta y^2 >= \frac{k_B T}{k_{\mathrm{mol}}} \quad . \tag{S2}$$

In this case the fluctuations of the position of the optical trap are expected to match those of the bead ($< \delta y^2 >$). However, in our experimental set-up a finite frequency feedback of 1 kHz is used (*i.e.* the force-feedback corrects the position of the optical trap by moving the piezoelectric actuators at a 1 kHz rate), and Eq. (S2) is not satisfied. To extract the value of k_{mol} we followed a phenomenological approach that uses a modified version of Eq. (S2) containing a proportionality constant c:

$$< \delta y^2 >= c\frac{k_B T}{k_{\mathrm{mol}}} \quad . \tag{S3}$$

The constant c includes all effects of the finite frequency of the feedback. The value of c has been obtained by fitting a set of measurements of ssDNA and dsDNA tethers at different average forces. The fluctuations in the position of the optical trap remain inversely proportional to k_{mol} in the investigated range of stiffness ($1 - 10 \cdot 10^{-3}$ pN/nm) (Figure S14**a**), verifying the validity of the method based on Eq. (S3). This calibration method has been used to estimate the changes in stiffness that KF induces in ssDNA. The stiffness of the molecule during the peptide flow is measured in short time-windows to ensure reliable measurements of $< \delta y^2 >$.

Data is recorded at 1 kHz and low frequencies are filtered out to remove instrumental drift as experiments run for long times (30 min). Filtering low frequencies is also important to correct the changes in extension due to the compaction of the DNA with KF. A time-window of 3 s has been found to be the optimal value to reduce drift without affecting the measurements (vertical dashed line in Figure S14**b**). Using a shorter time-window removes fluctuations that are relevant to determine the stiffness of the tether due to the large autocorrelation time shown by the data (Figure S14**c**).

S5 Elastic properties of ssDNA before incubation with KF

Before flowing KF, pulling curves of the ssDNA molecule were recorded. The relative molecular extension was determined by subtracting the trap compliance (F/k) to the absolute displacement of the optical trap (trap stiffness: 70 pN/μm). To obtain the absolute molecular extension, the elastic response of the tethered molecule was aligned to a reference unzipping trajectory in the range of forces from 15 to 20 pN (ssDNA response of the molecule). This method allowed to accurately calibrate the absolute extension of the molecule within less than 50 nm.

The method used to prepare the ssDNA template leaves a very short dsDNA stretch (88-bp) in relation to the length of the ssDNA chain (13650 bases). As the rigidity of dsDNA is $\sim$70-fold that of ssDNA, pulling curves mainly reflect the elastic response of the ssDNA region. At a given salt concentration, pulling curves of ssDNA can be modeled with the Freely-Jointed Chain (FJC) model:[S1]

$$x(F) = d_0 N_b \left[\frac{1}{\tanh(\frac{Fb}{k_b T})} - \frac{k_b T}{Fb} \right] \tag{S4}$$

where: b: Kuhn length , d_0: Interphosphate distance, N_b: Number of bases.

Pulling curves were fitted to the FJC model finding average values of $b = 1.57 \pm 0.05$ nm and d_0=0.57 $\pm$ 0.03 nm (N=5), compatible with previously reported results for the same ionic condition.[S1,S7] Data was fitted on the force-range 5-25 pN, as experiments were performed at a salt concentration ([NaCl]=100 mM) at which secondary structure formation is not observed at low forces.

S6 Supplementary Figures

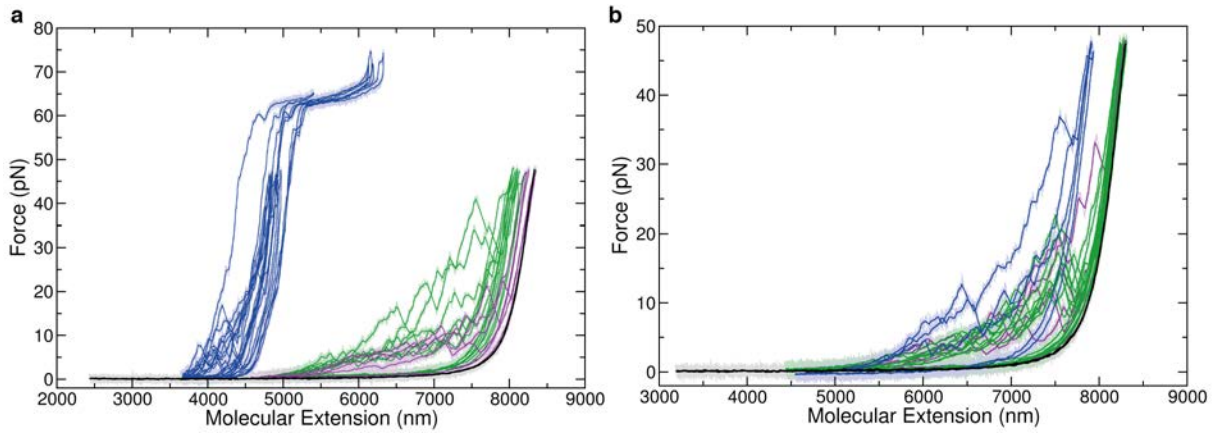

Figure S1: **Reproducibility of KF-DNA force-extension curves.** (**a**) Pulling cycles of a 24-kb DNA molecule before (black) and after flowing 40 μM KF at different waiting times: 5 min (purple), 15 min (green), 30 min (blue). (**b**) Pulling cycles of a 24-kb DNA molecule before (black) and after incubation with 40 μM KF at different waiting times of the interaction: 5 min (purple), 15 min (green), 30 min (blue). Similar trends to those reported in Figure 2**a** are seen. Raw data was obtained at 1 kHz acquisition rate (light colors) and filtered to 10 Hz bandwidth (dark colors). Pulling speed is 500 nm/s.

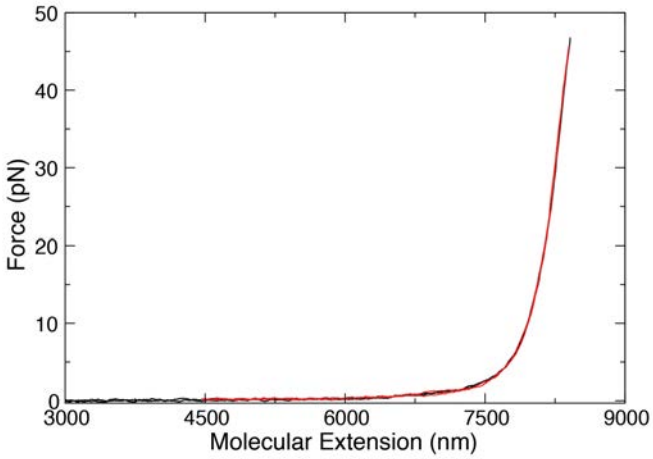

Figure S2: **The ornithine residue is essential for DNA binding.** Stretching curves of a 24-kb DNA molecule before (black) and after (red) flowing a KF analog (40 μM) in which the ornithine residue has been replaced by a glutamic acid. The characteristic sawtooth pattern induced by KF is not observed, and compatible values for the elastic parameters are found if force-extension curves are fitted to the WLC model before and after flowing the analog. Data is filtered at 10Hz bandwidth.

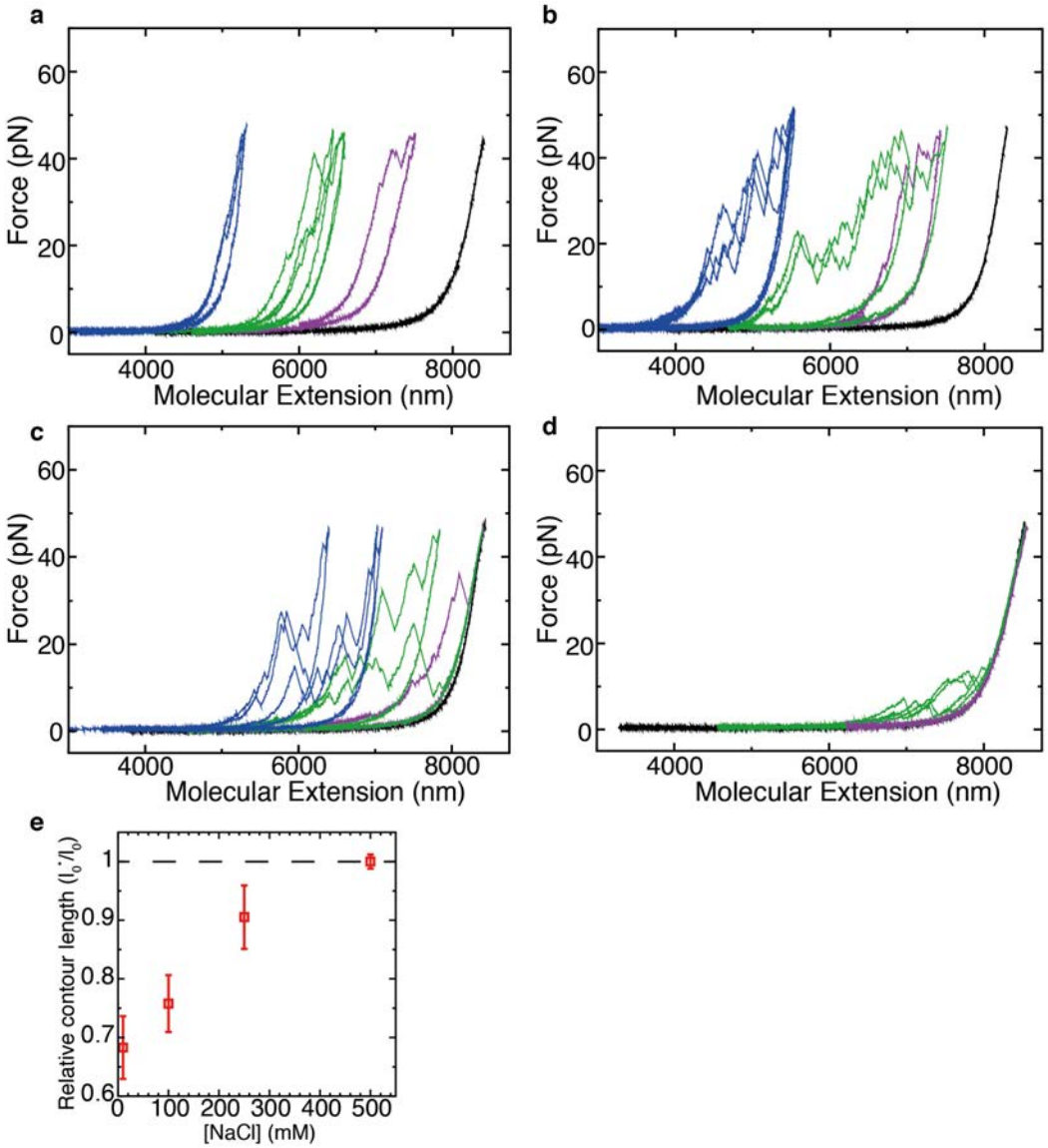

Figure S3: **Effect of ionic strength on KF-DNA interaction. (a) 10 mM NaCl. (b) 100 mM NaCl. (c) 250 mM NaCl. (d) 500 mM NaCl.** In panels (a-d) we show representative experiments at each salt condition in which a DNA molecule is pulled before (black) and after flowing 10 μM KF (color). After flowing the peptide, the DNA molecule was repeatedly pulled between a maximum force of 45 pN and a minimum extension of 6 μm (purple), 4 μm (green) and 3 μm (blue). At the highest ionic strength (500 mM NaCl) we did not observe binding of the peptide to DNA, except for one experiment in which we obtained the results shown in panel d (green curve). Data is filtered at 50 Hz bandwidth, pulling speed v=500 nm/s. We performed at least 5 experiments at each condition. (e) Apparent contour length of the DNA molecule ($l_0{}^*$) relative to its original extension (l_0=8.3 μm), after being repeatedly pulled between a maximum force of 45 pN and a minimum extension of 4 μm. The degree of compaction of the DNA molecule increases with decreasing ionic strength (mean$\pm$SD, N=5, except for 500 mM in which we only observed binding in one experiment).

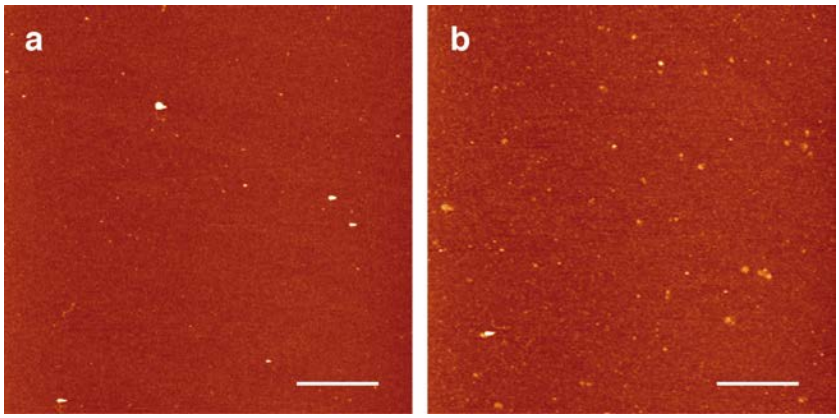

Figure S4: **AFM imaging of KF in the absence of DNA.** (**a**) 100 μM KF immediately after dilution in aqueous buffer. (**b**) 100 μM KF incubated for 30 min at room temperature. Aggregation spots are occasionally observed on the surface at both incubation times. Bar scale is 600 nm. Color scale (from dark to bright) is 0-2 nm in all AFM images.

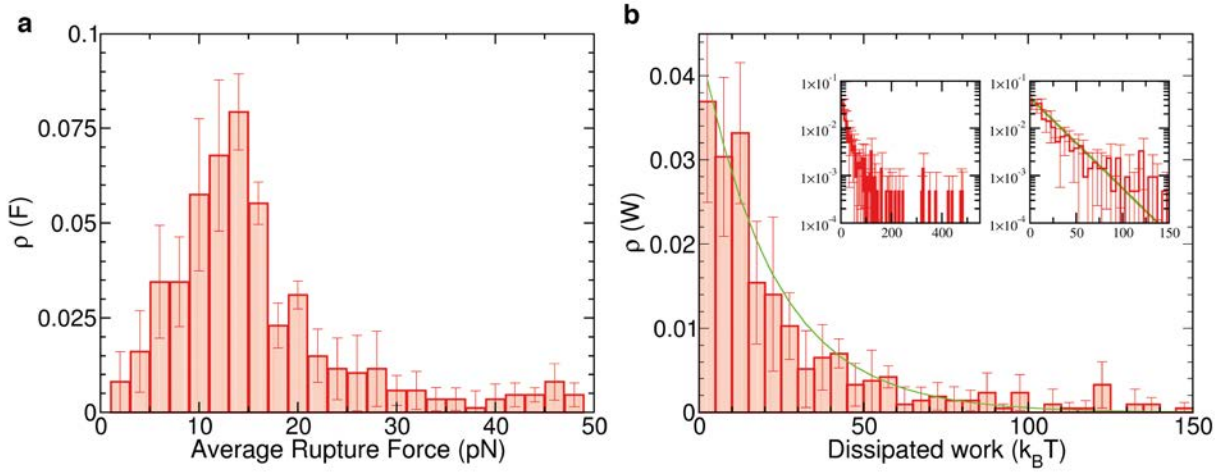

Figure S5: **Analysis of KF-DNA unpeeling events** (**a**) Average rupture force of KF-DNA contacts. The average rupture force is calculated as the mean of the average force immediately before and after an unpeeling event (**b**) Histogram of dissipated work in individual unpeeling events (calculated using equation (2) in main text). The histogram follows an exponential distribution of mean 23 ± 8 k_BT (green). A rightmost tail corresponding to individual unpeeling events with $W_{\text{dissipated}} \geq 150$ k_BT is observed. Insets show a log-normal plot (right) and the same plot with an enlarged range of $W_{\text{dissipated}}$ values (left). Unpeeling events with dissipated work as large as 400 k_BT are observed. For both figures N=435 events from 3 molecules. Error bars are the statistical error measured between different molecules.

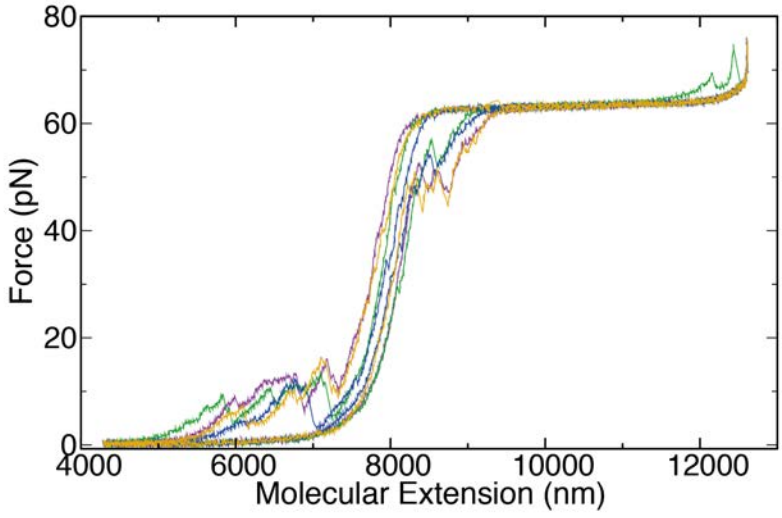

Figure S6: **KF binding does not change the overstretching transition.** Four consecutive stretching curves (purple, green, blue and yellow) of a 24-kb DNA molecule after incubation with 50 μM KF. The molecule is fully overstretched at each pulling cycle. The sawtooth pattern at low extensions is clearly visible at each cycle. Data was filtered at 100 Hz bandwidth, v=1000 nm/s.

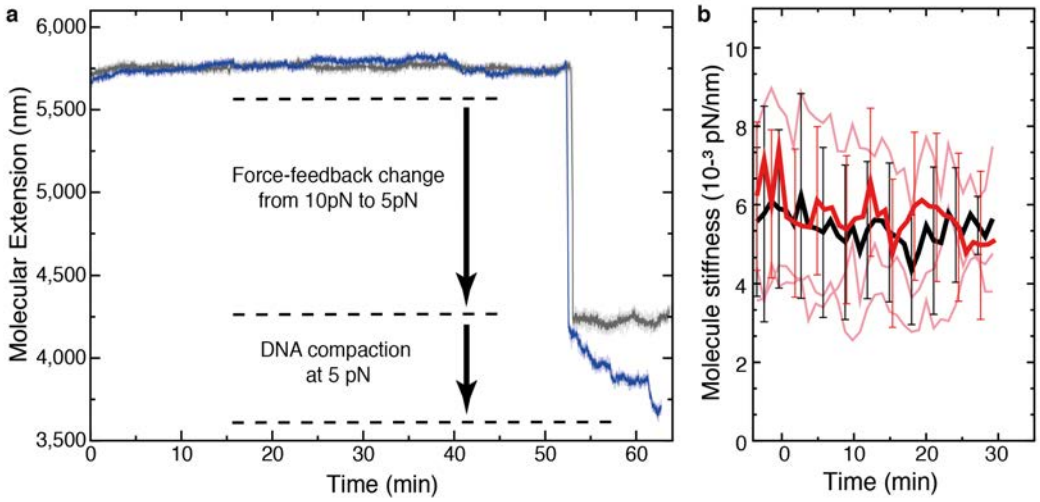

Figure S7: **KF compacts ssDNA at 5 pN but not at 10 pN** (**a**) A ssDNA molecule is maintained for more than 50 min at a constant force of 10 pN with a flow of KF, without observing a significant decrease in extension (blue). However, when the force is lowered to 5 pN (top arrow) a compaction equivalent to that reported in Figure 7**b** is seen (bottom arrow). A negative control without peptide in the flowed buffer does not show DNA compaction (gray). Raw data is obtained at 1 kHz (light colors) and filtered at 1 Hz bandwidth (dark colors). (**b**) Average stiffness of ssDNA at 10 pN during the first 30 min of the peptide flow (red) compared to a negative control without peptide (black). Three individual experiments are shown in light red. In contrast to the results shown in Figure 7**b**, the molecular stiffness remains constant in time.

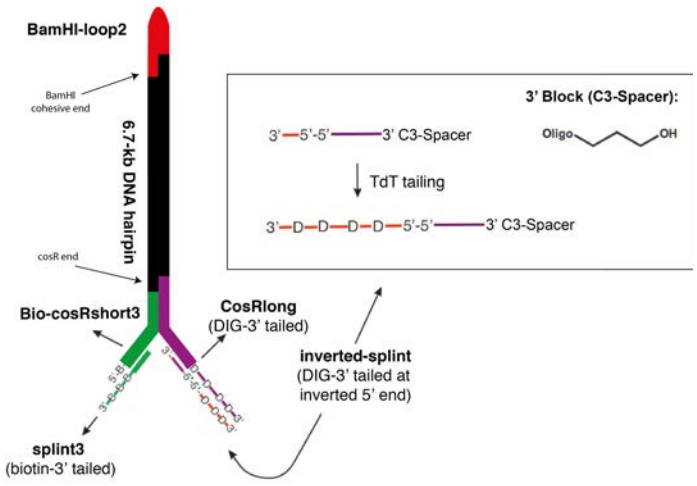

Figure S8: **Scheme of the DNA hairpin synthesis.** The DNA hairpin is created by ligating a set of oligonucleotides (red, green, purple) to a 6.7-kb restriction fragment of λ-DNA (black). The cosR end, and an *Xba*I cohesive end were respectively used to anneal the dsDNA handles and the end-loop to the λ-DNA fragment. To create the biotinylated handle (green) one oligonucleotide was purchased 5'-biotinlylated (Bio-cosRshort3) and the other one was tailed with multiple biotins at its 3' end (splint3). To create a dsDNA handle with multiple digoxigenins at each strand we used an oligonucleotide containing a 5'-5' inversion and a blocked 3' end (inverted-splint). In this way the two oligonucleotides that create this handle (cosRlong, inverted-splint) could be tailed with multiple digoxigenins at the appropriate end.

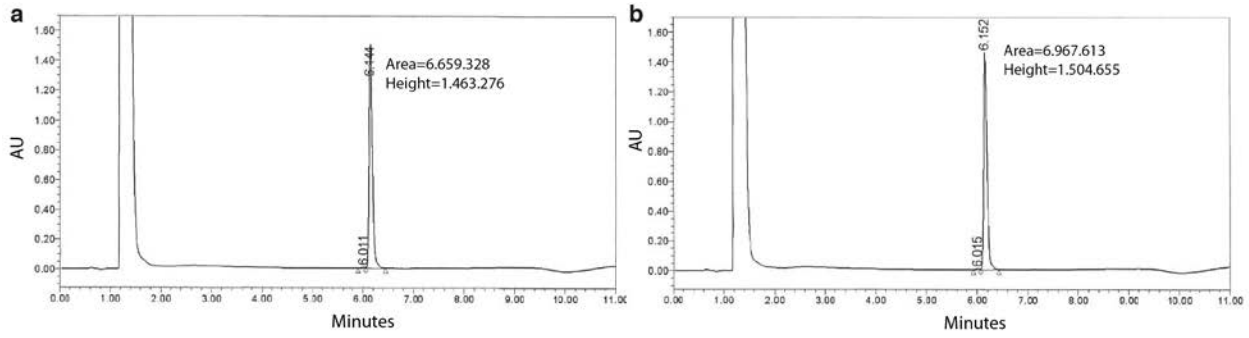

Figure S9: **KF stock filtration does not reduce sample concentration** (**a**) Chromatogram of a freshly dissolved 2 mM KF stock solution before filtration (wavelength: 220 nm). The elution peak of KF is seen at t=6.4 min. (**b**) Chromatogram of a freshly dissolved 2 mM KF stock solution after filtration. The elution peak of KF is seen at t=6.5 min. The area and height of the filtered and non-filtered samples are comparable, indicating that KF concentration is not reduced due to filtration. The high peak at t=1 min corresponds to DMSO.

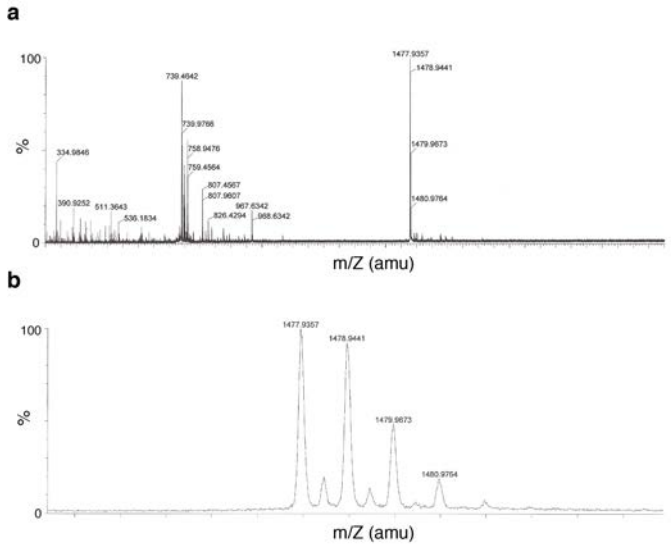

Figure S10: **Mass spectrometry of Kahalalide F** (**a**) Mass spectrum of a 40 μM KF sample. Peaks found at 1478 m/Z correspond to the singly charged ion and doubly charged dimer. The peaks at 967 m/Z and 511 m/Z correspond to a fragmentation reaction of the peptide at D-val/D-Pro.[S8] (**b**) Zoom of the main peak of the mass spectrum from (a).

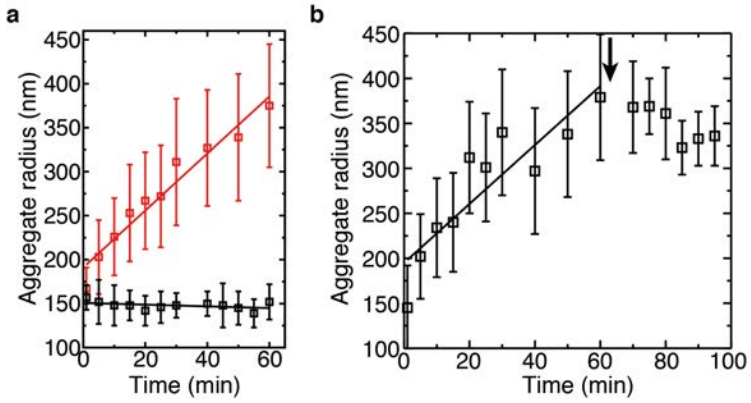

Figure S11: **DLS measurements of KF and KF-DNA complexes. (a) (red)** Hydrodynamic radius of KF particles in the buffer used for optical tweezers experiments (40 μM KF, 25°C, mean±SD, N=9). KF forms nanometer-sized aggregates whose size grows linearly with time. The aggregation rate is obtained from a linear fit (red line). Significant differences are not seen between KF stock aliquots stored at $-20°C$ or solutions freshly prepared from lyophilized KF. **(black)** Hydrodynamic radius of KF aggregates when DNA is added to the sample immediately after dilution (KF 40 μM, 48-kb λ-DNA 6.25 μg/ml, 25°C, mean±SD, N=3). The size of the KF aggregates remains constant up to 1 hour after dilution, showing that DNA has a stabilizing effect on the size of the aggregates. A linear fit is shown in black. **(b)** The size of the KF aggregates (black) can also be stabilized by adding DNA (arrow) after 60 min (mean±SD, N$\geq$3). A linear fit is shown to highlight the stabilization of the particle size after adding DNA.

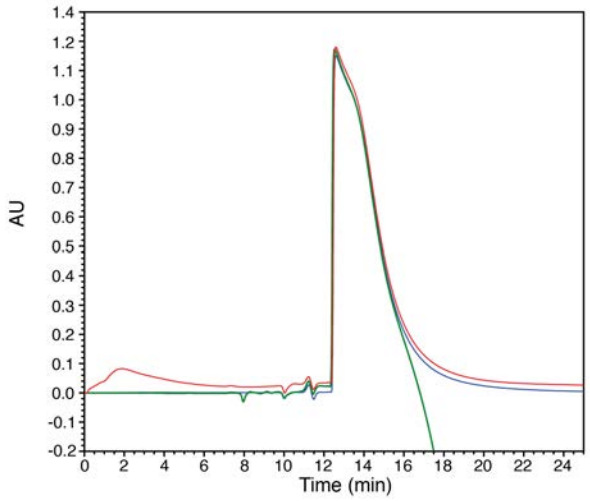

Figure S12: **Aggregation of KF dilutions.** Size-exclusion chromatography of 40μM KF dilutions at different waiting times: immediately after dilution (blue), after 30 min (green) and after 3 h (red). The width of the elution peak indicates peptide aggregation at all times.

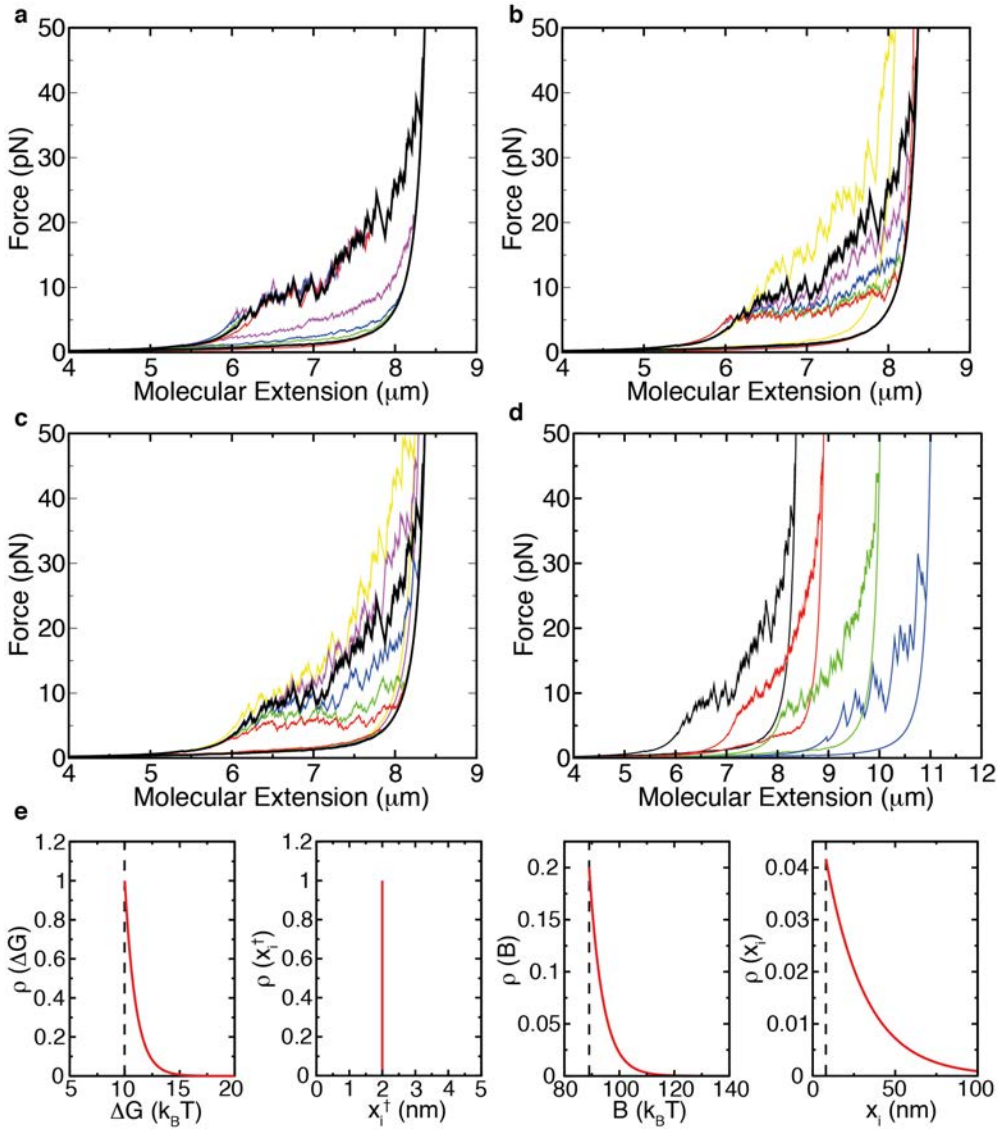

Figure S13: **Simulations of KF-DNA stretching experiments.** (**a**) Simulations varying ΔG_0 (minimum value of the exponential distribution of ΔG values, width $w = 1\ k_BT$): ΔG_0=5 k_BT (red), ΔG_0=10 k_BT (black, optimal value), ΔG_0=15 k_BT (green), ΔG_0=20 k_BT (blue), ΔG_0=40 k_BT (purple). (**b**) Simulations varying $x_i^\dagger$: $x_i^\dagger$=10 nm (red), $x_i^\dagger$=8 nm (green), $x_i^\dagger$=5 nm (blue), $x_i^\dagger$=3 nm (purple), $x_i^\dagger$=2 nm (black, optimal value), $x_i^\dagger$=1 nm (yellow). (**c**) Simulations varying w' (exponential tail of the barrier B): w'=0 k_BT (red), w'=1 k_BT (green), w'=3 k_BT (blue), w'=5 k_BT (black, optimal value), w'=7 k_BT (purple), w'=10 k_BT (yellow) (**d**) Simulations varying x_i (contact-length distribution): experimental distribution $p(x_i) = (1/w)\exp[-(x_i - x_{i,0})/w]$ for $x_i \geq x_{i,0}$ ($p(x_i)$=0 otherwise) with $x_{i,0}$=8 nm and w=24 nm (black), x_i= 10 nm (red), x_i=30 nm (green), x_i=100 nm (blue). Simulations are shifted by 1 μm for clarity. (**e**) Optimal distributions for the different parameters of the simulation (corresponding to the black lines in panels a-d).

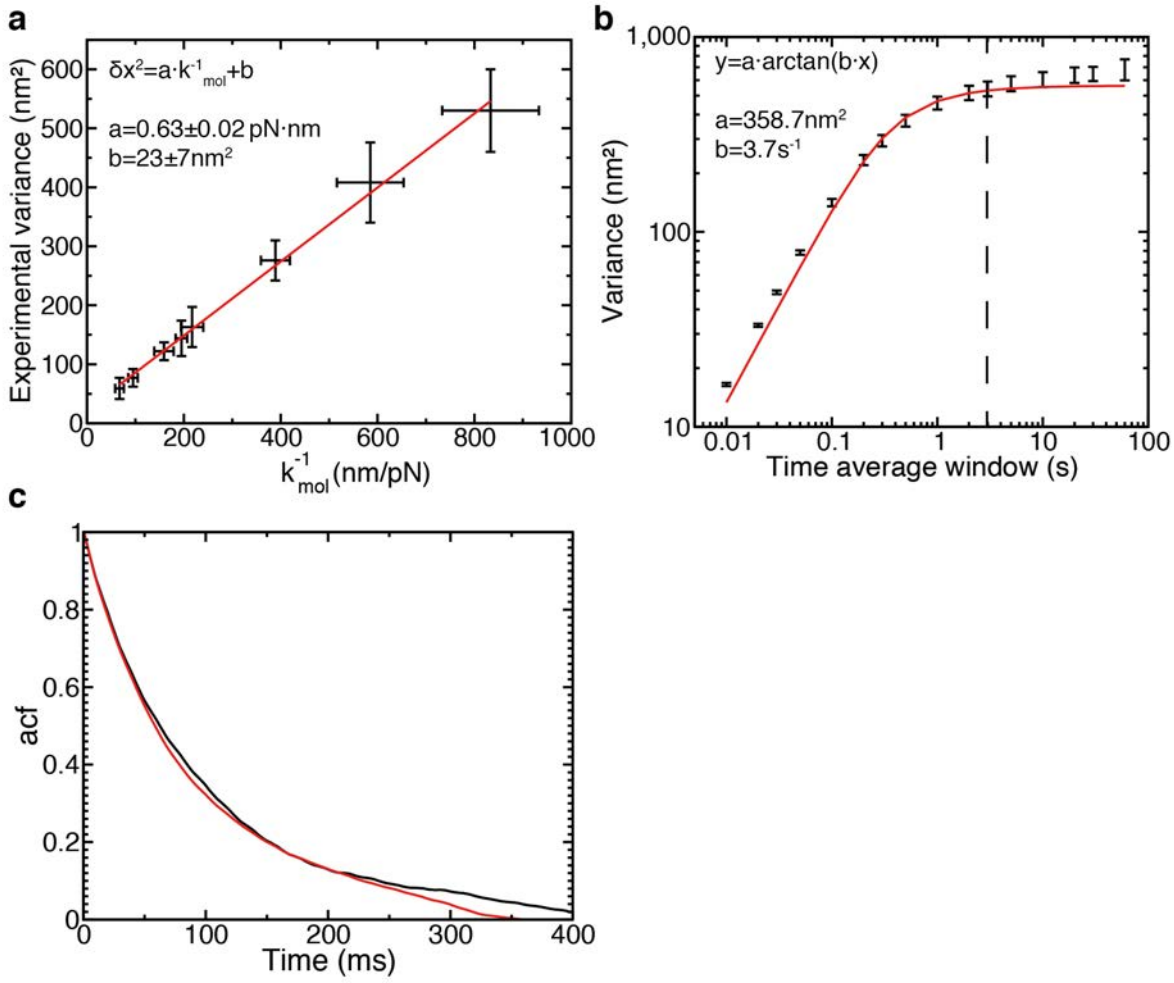

Figure S14: **Stiffness determination from trap-position fluctuations.** (**a**) Phenomenological calibration of the molecular stiffness. The experimental variance of the trap position for a set of ssDNA and dsDNA molecules at different average forces was measured with the force-feedback protocol. The stiffness of the molecule (k_{mol}) was determined as the derivative of the force-extension curve at each force. (**b**) Drift correction of the experimental data. The position of the trap is recorded at 1 kHz, and drift is removed by subtracting the average position using time-windows in the range 0.01-60 s (black). A window of 3 s (dashed line) is the optimal value to remove drift without distorting the measurement of the fluctuations. Data is fitted to an arctangent function (red). Measurements correspond to a 13-kb ssDNA molecule at 5 pN (N=5). (**c**) Autocorrelation function of the distance during two constant force experiments at 8 pN for a ssDNA molecule after subtracting the drift. Data with (red) and without (black) a buffer flow are shown.

S7 Supplementary Tables

Table S1: **Zeta potential measurements.** Zeta pontential of KF (40 μM) and λ-DNA (6.25 μg/ml, 0.2 nM) solutions as well as their mixtures in water at 25$^{\circ}C$ (mean$\pm$SD, N$\geq$3). KF aggregates in water have a slighlty positive zeta potential -too low to prevent aggregation-, but suggesting that peptide aggregates might preferentially expose the positively charged residues on the surface. The addition of DNA to the sample shifts the zeta potential to negative values, further supporting that DNA binds to the peptide aggregates preventing their growth.

	Zeta Potential (mV)	Electrophoretic Mobility ($\mu m \cdot$cm$\cdot$V$\cdot s^{-1}$)
KF	7.3 ± 0.3	0.6 ± 0.1
DNA	-46.1 ± 5.5	-3.4 ± 0.3
DNA/KF	-30.1 ± 1.2	-2.4 ± 0.1

Table S2: **Oligonucleotides used for the DNA hairpin synthesis and to generate the ssDNA template.**

Oligonucleotide name	Oligonucleotide sequence
BamHI-loop II	5'-GATCGCCAGTTCGCGTTCGCCAGCATCCG ACTACGGATGCTGGCGAACGCGAACTGGC-3'
cosRlong	5'-Pho-GGGCGGCGACCTAAGATCTATTATATATGTG TCTCTATTAGTTAGTGGTGGAAACACAGTGCCAGCGC-3'
BIO-cosRshort3	5'-Bio-GACTTCACTAATACGACTCACTATAGGG AAATAGAGACACATATATAATAGATCTT-3'
splint3	5'-TCCCTATAGTGAGTCGTATTAGTGAAGTC-3'
inverted-splint	3'-AAAAA-5'-5'-GCGCTGGCACTGTGTTTCCACCACTAAC(SpC3)-3'
Blockloop30	5'-TAGTCGGATGCTGGCGAACGCGAACTGGCG-3'

References

[S1] Huguet, J. M.; Bizarro, C. V.; Forns, N.; Smith, S. B.; Bustamante, C.; Ritort, F. Single-Molecule Derivation of Salt Dependent Base-Pair Free Energies in DNA. *Proc. Natl. Acad. Sci. U.S.A.* **2010**, *107*, 15431–15436.

[S2] Borchardt, R.; Kerns, E.; Lipinski, C.; Thakker, D.; Wang, B. *Pharmaceutical Profiling in Drug Discovery for Lead Selection*; American Assoc. of Pharm. Scientists, 2005; Vol. 1.

[S3] Kozikowski, B. A.; Burt, T. M.; Tirey, D. A.; Williams, L. E.; Kuzmak, B. R.; Stanton, D. T.; Morand, K. L.; Nelson, S. L. The Effect of Freeze/Thaw Cycles on the Stability of Compounds in DMSO. *J. Biomol. Screening* **2003**, *8*, 210–215.

[S4] McDonald, G. R.; Hudson, A. L.; Dunn, S. M. J.; You, H.; Baker, G.; Whittal, R.; Martin, J.; Jha, A.; Edmondson, D. E.; Holt, A. Bioactive Contaminants Leach from Disposable Laboratory Plasticware. *Science* **2008**, *322*, 917.

[S5] Nuijen, B.; Bouma, M.; Manada, C.; Jimeno, J. M.; Lazaro, L.; Bult, A.; Beijnen, J. Compatibility and Stability of the Investigational Polypeptide Marine Anticancer Agent Kahalalide F in Infusion Devices. *Invest. New Drugs* **2001**, *19*, 273–281.

[S6] Forns, N.; De Lorenzo, S.; Manosas, M.; Hayashi, K.; Huguet, J.; Ritort, F. Improving Signal/Noise Resolution in Single-Molecule Experiments Using Molecular Constructs with Short Handles. *Biophys. J.* **2011**, *100*, 1765–1774.

[S7] Smith, S.; Cui, Y.; Bustamante, C. Overstretching B-DNA: the Elastic Response of Individual Double-Stranded and Single-Stranded DNA Molecules. *Science* **1996**, *271*, 795–799.

[S8] Stokvis, E.; Rosing, H.; Lopez-Lazaro, L.; Rodriguez, I.; Jimeno, J.; Supko, J.; Schellens, J. H. M.; Beijnen, J. H. Quantitative Analysis of the Novel Depsipeptide Anticancer Drug Kahalalide F in Human Plasma by High-Performance Liquid Chromatography under Basic Conditions Coupled to Electrospray Ionization Tandem Mass Spectrometry. *J. Mass Spectrom.* **2002**, *37*, 992–1000.